

SCASeg: Strip Cross-Attention for Efficient Semantic Segmentation

Guoan Xu¹, Jiaming Chen², Wenfeng Huang¹, Wenjing Jia¹, Guangwei Gao³, and Guo-Jun Qi⁴
¹University of Technology Sydney, Australia ²University of Manchester, UK
³Nanjing University of Posts and Telecommunications, China ⁴Westlake University, China

Abstract

The Vision Transformer (ViT) has achieved notable success in computer vision, with its variants extensively validated across various downstream tasks, including semantic segmentation. However, designed as general-purpose visual encoders, ViT backbones often overlook the specific needs of task decoders, revealing opportunities to design decoders tailored to efficient semantic segmentation. This paper proposes Strip Cross-Attention (SCASeg), an innovative decoder head explicitly designed for semantic segmentation. Instead of relying on the simple conventional skip connections, we employ lateral connections between the encoder and decoder stages, using encoder features as Queries for the cross-attention modules. Additionally, we introduce a Cross-Layer Block that blends hierarchical feature maps from different encoder and decoder stages to create a unified representation for Keys and Values. To further boost computational efficiency, SCASeg compresses queries and keys into strip-like patterns to optimize memory usage and inference speed over the traditional vanilla cross-attention. Moreover, the Cross-Layer Block incorporates the local perceptual strengths of convolution, enabling SCASeg to capture both global and local context dependencies across multiple layers. This approach facilitates effective feature interaction at different scales, improving the overall performance. Experiments show that the adaptable decoder of SCASeg produces competitive performance across different setups, surpassing leading segmentation architectures on all benchmark datasets, including ADE20K, Cityscapes, COCO-Stuff 164k, and Pascal VOC2012, even under varying computational limitations.

1. Introduction

Semantic segmentation is a fundamental task in computer vision that involves pixel-level classification [8, 28, 30, 47, 49]. This process entails labeling each pixel in an image to accurately identify object categories, spatial positions, and other critical information, thereby providing a detailed understanding of the scene’s composition. Semantic seg-

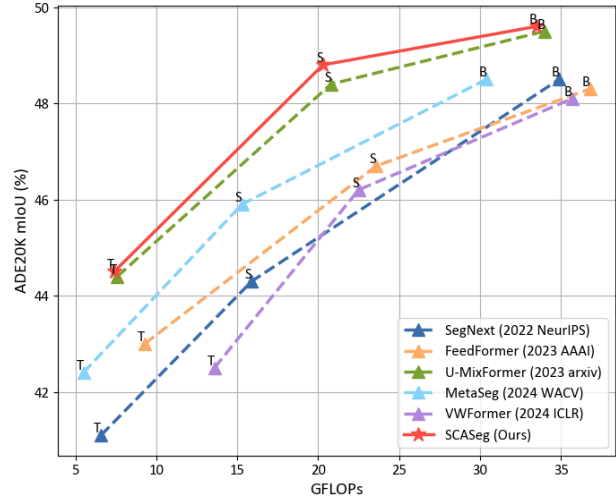


Figure 1. The mIoU and GFLOPs comparisons of SCASeg with SOTA approaches on ADE20K [53], reported using a single model and single-scale inference based on MSCAN [16] backbones.

mentation has widespread applications in various fields, including autonomous driving [39], medical diagnosis [2], and remote sensing [35], among others [21, 22]. A pivotal development in this area was the introduction of the fully convolutional network (FCN) [27], which popularized the encoder-decoder architecture. In this architecture, the encoder extracts high-level semantic features while the decoder integrates these features with spatial details. Despite subsequent advancements [14], traditional CNNs still struggle to capture long-range dependencies effectively.

This limitation has been largely addressed with the emergence of Transformers [33]. Following its groundbreaking success in Natural Language Processing (NLP), the Transformer quickly began to make a significant impact on vision tasks as well. Its self-attention mechanism is highly effective at capturing long-range dependencies within input sequences. Dosovitskiy *et al.* [13] extended this concept to the visual domain by proposing the Vision Transformer (ViT) backbone, which involves dividing images into small patches, transforming them into one-dimensional sequences, and feeding these sequences into the Transformer encoder to align the input dimensions for visual pro-

cessing. However, most of these approaches have focused primarily on optimizing the efficiency of the Transformer encoder while relying on simple or pre-existing designs for the decoder architecture. For instance, Segformer [38] emphasizes designing an efficient Transformer encoder while utilizing a straightforward all-MLP decoder. Similarly, SegNeXt [16] develops a lightweight and efficient backbone but adopts a simplistic approach in the decoder stage.

More recently, MetaSeg [20] introduced a new and efficient self-attention module called Channel Reduction Attention (CRA), which simplifies the channel dimensions of the query and key into a single dimension per head within the self-attention process. However, this approach does not effectively facilitate interaction among the various feature representations. Feedformer [31] adopts a strategy of utilizing features directly as queries, rather than relying on class-specific learnable queries. U-MixFormer [44] adaptively incorporates multi-stage features as keys and values within its specialized mix-attention module. MacFormer [40] introduces a mutual agent cross-attention mechanism to enhance bidirectional feature interaction. Additionally, it proposes detailed enhancement in the frequency domain, achieving notable results. Despite the advancements offered by these attention blocks, they do not adequately consider the importance of local information. As demonstrated by models such as Metaformer [46], CMT [15], SMT [24], and XcIT [1], convolution methods are more effective than Transformers in capturing local features. Therefore, it is crucial to integrate local perception capabilities into the model alongside global attention mechanisms.

Based on the above observations and considerations, and in pursuit of a balance between efficiency and performance, we propose a novel Cross-Layer Block that consists of the designed cross-attention module called *Strip Cross-Attention (SCA)* and a *Local Perception Module (LPM)*. Specifically, SCA is responsible for managing global long-range context dependencies, while LPM focuses on extracting local feature information. This combination achieves a better trade-off between efficiency and effectiveness (Fig. 1 shows some comparisons). In summary, the main contributions of our method are summarized as follows.

1. We present an innovative and robust transformer-decoder architecture designed for efficient semantic segmentation. Building on U-Net’s strengths in capturing and transmitting hierarchical features, our approach uniquely utilizes lateral connections from the transformer encoder as query features.
2. We introduce a meticulously designed Cross-Layer Block consisting of two key modules: Strip Cross-Attention and the Local Perception Module. These modules work together to capture both local and global contexts effectively.
3. Comprehensive experiments were conducted using var-

ious backbones on benchmark datasets, including ADE20K, Cityscapes, COCO-Stuff 164k, and Pascal VOC2012, resulting in SOTA performance.

2. Related Work

2.1. Semantic Segmentation

Semantic segmentation can be seen as an evolution of image classification, transitioning from categorizing entire images to assigning labels at the pixel level [9, 25, 37, 41, 51]. During the deep learning era, the Fully Convolutional Network (FCN) [27] marked a significant breakthrough in semantic segmentation by utilizing a fully convolutional architecture for end-to-end pixel-wise classification. Following the development of FCN, researchers focused on enhancing it from various perspectives, such as, 1) Enlarging the receptive field [7, 23, 29]: DeepLab-v3 [6] introduced dilation rates in the Atrous Spatial Pyramid Pooling (ASPP) module, allowing for a larger and more multi-scale receptive field. 2) Improving contextual information [17, 45, 49]: CPNet [45] enhances feature learning accuracy by encoding ground truth into a one-hot representation and introducing a context prior to the encoder, which provides more precise guidance for feature learning. 3) Incorporating boundary information [12, 48, 50]: BPKD [26] employs edge detection operators to dilate and erode the target object, effectively extracting their edges, and uses knowledge distillation to transfer accurate edge information from a teacher model to a student network. 4) Designing various attention mechanisms [14, 19, 36, 52]: DANet [14] and CCNet [19] extend non-local attention by integrating channel attention concepts to enhance overall model performance. Although these approaches have significantly improved semantic segmentation performance, they have also introduced numerous empirical modules, resulting in computationally intensive and complex frameworks.

2.2. Decoder Head

For semantic segmentation, Segmenter [32] leverages the output embeddings associated with image patches and retrieves class labels from these embeddings using either a point-wise linear decoder or a mask transformer decoder. MetaSeg [20] introduces a lightweight decoder module called Channel Reduction Attention, which enables self-attention in each stage’s output while reducing computational load. However, a limitation is the lack of cross-layer interaction, indicating potential areas for improvement. FeedFormer [31] enhances efficiency by taking high-level encoder features as queries and the lowest-level encoder features as keys and values. Nevertheless, this method processes feature maps independently without progressive propagation across decoder stages, missing opportunities for gradual refinement that could enhance object bound-

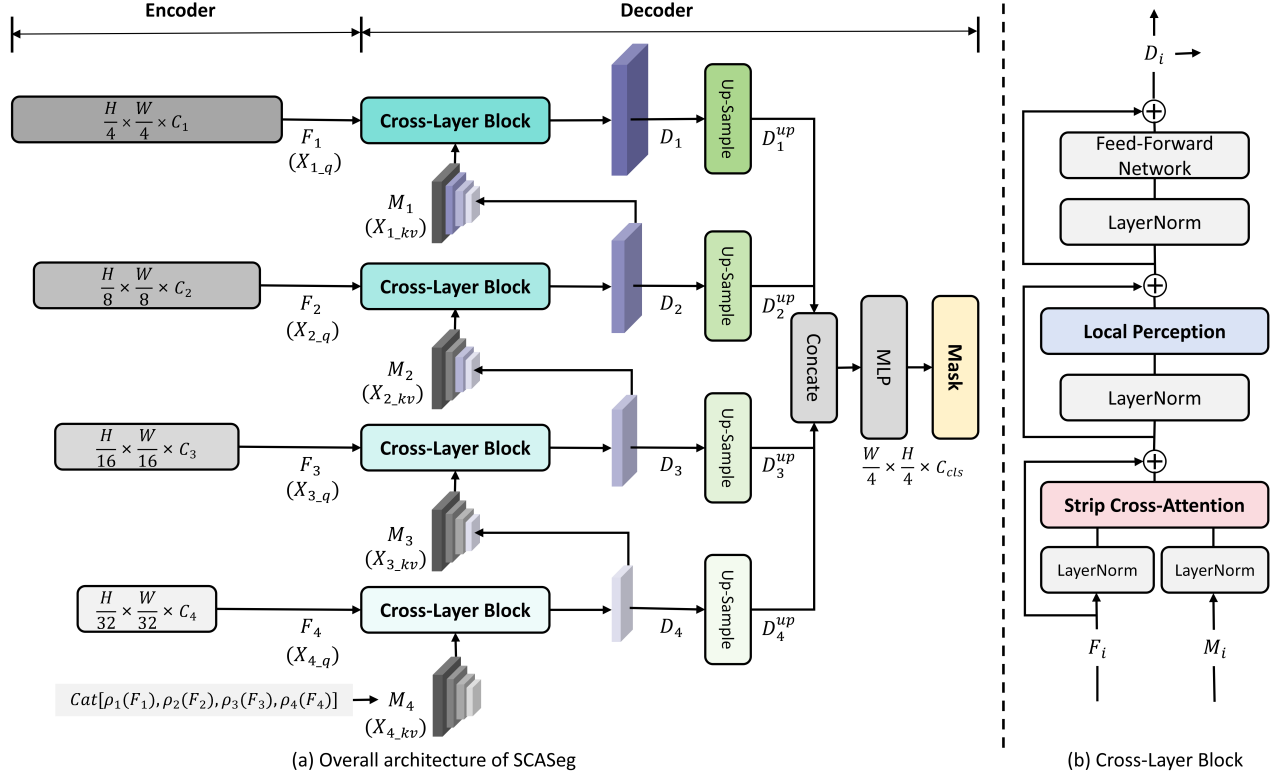


Figure 2. The overall architecture of our proposed SCASeg and Cross-Layer Block (CLB).

ary detection. UMixFormer [44] introduces a mix-attention mechanism that first downsamples features from different levels and concatenates them to form queries. Features from each encoder level are then treated as keys and values, with cross-attention applied progressively across layers. The newly generated feature map is merged back into the original concatenated features to form new queries.

3. Proposed Method

3.1. Overall Architecture

As illustrated in Fig. 2 (a), our SCASeg framework is compatible with any pretrained model that features a hierarchical four-stage architecture. This work employs lightweight backbones such as MiT-B0~B5 and MSCAN-T/S/B as encoders, efficiently extracting rich feature representations. Inspired by U-Mixformer [44], we have developed a refined version of the U-Net structure for the decoder. This enhanced design integrates a Cross-Layer Block to facilitate inter-level feature interaction with a low computational burden, significantly improving decoding capability.

Given an image I of size $H \times W \times 3$ as input, feature maps $F_i \in \mathbb{R}^{\frac{H}{2^{i+1}} \times \frac{W}{2^{i+1}} \times C_i}$ are extracted at each stage of the encoder, where $i \in \{1, 2, 3, 4\}$ indicates the corresponding encoder stage and C_i denotes the number of channels in that stage. These features provide a progression from coarse to fine detail, contributing to the improved performance of

semantic segmentation.

The decoder in our SCASeg utilizes the U-Net architecture to better capture global contexts that are insufficiently addressed by the encoder. At each stage of the decoder, refined features D_i are progressively generated through the Cross-Layer Block, where the query features X_q^i correspond to the respective lateral encoder feature maps F_i . The key and value feature X_{kv}^i (denoted as M_i in Fig. 2) is derived from a combination of both encoder and decoder stages. The decoder features are then upsampled using bilinear interpolation to match the height and width of D_1 . Finally, the concatenated features are passed through an MLP to generate the segmentation masks with dimensions of $\frac{H}{4} \times \frac{W}{4} \times 3$.

The entire decoding process can be summarized as

$$M_i = \text{Cat}[\rho_1(F_1), \dots, \rho_i(F_i), D_{i+1}, \dots, D_4]_{i=1}^4, \quad (1)$$

$$D_i = \text{CLB}(F_i, M_i), \quad (2)$$

$$D_i^{up} = \text{Up}(D_i, 2^{i-1}), \quad (3)$$

$$O_{mask} = \text{MLP}(\text{Cat}[D_i^{up}]_{i=1}^4), \quad (4)$$

where Cat denotes the concatenation operation, ρ represents a downsampling pooling operation, CLB stands for Cross-Layer Block, and Up refers to an upsampling function, which includes the scaling factor. The MLP is implemented using linear functions.

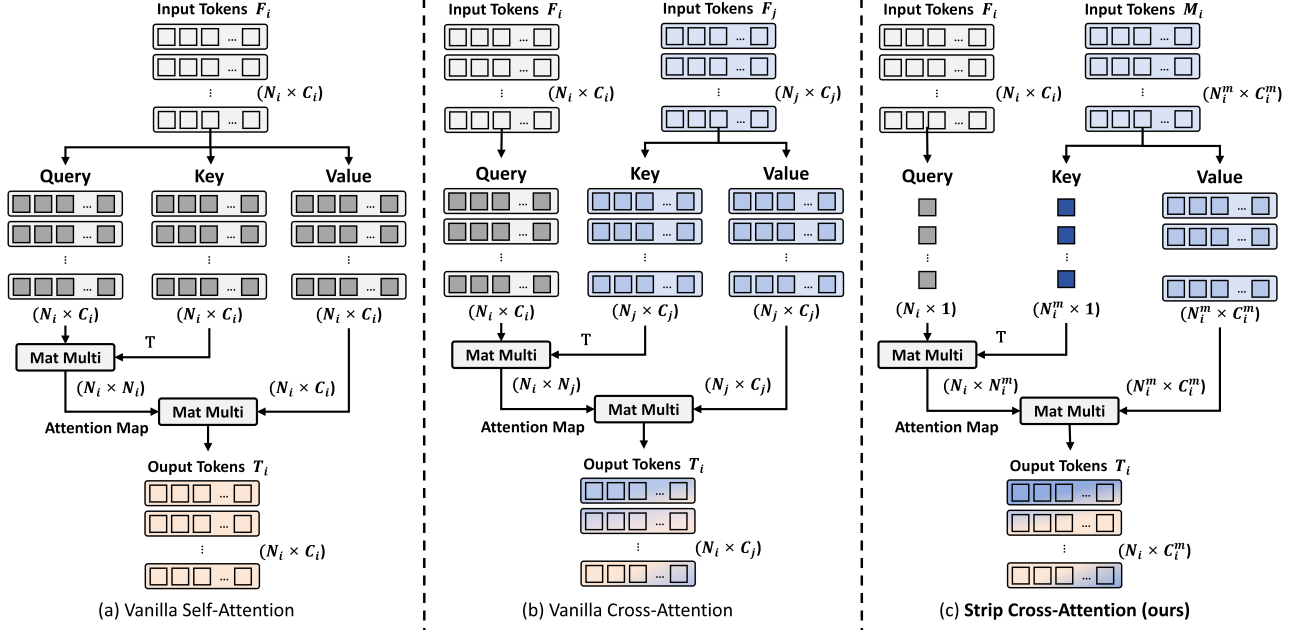


Figure 3. The proposed Strip Cross-Attention in comparison with the vanilla Self-Attention and Cross-Attention.

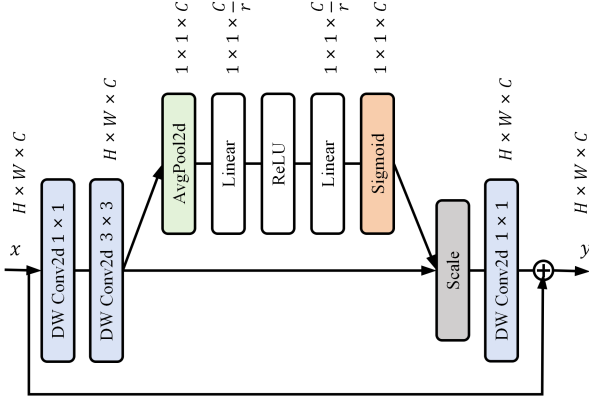


Figure 4. The architecture of our Local Perception Module (LPM).

3.2. Cross-Layer Block (CLB)

The proposed Cross-Layer Block (CLB) incorporates the MetaFormer [46] block in the decoder to enhance the global context of the feature representations extracted by the encoder, with a primary focus on integrating contextual information across different hierarchical features.

As illustrated in Fig. 2 (b), the CLB includes the MetaFormer block, which consists of three residual sub-blocks, a local perception module, and a novel Strip Cross-Attention (SCA) module for token mixing. The SCA module effectively captures both local and global contexts of the features while seamlessly integrating information across different hierarchical levels with minimal computational cost. The CLB is applied at each stage, taking two distinct inputs, F_i and M_i .

Thus, the entire process is defined as follows:

$$Z_i^G = SCA(LN(F_i), LN(M_i)) + F_i, \quad (5)$$

$$Z_i^{GL} = LPM(LN(Z_i^G)) + Z_i^G, \quad (6)$$

$$D_i = MLP(LN(Z_i^{GL})) + Z_i^{GL}, \quad (7)$$

where SCA and LPM stand for the Strip Cross-Attention (SCA) and Local Perception Module (LPM) operations. Z_i^G captures global features, whereas Z_i^{GL} fuses both local and global contexts. Layer Normalization (LN) is employed to standardize these features.

3.3. Strip Cross-Attention (SCA)

We introduce the Strip Cross-Attention (SCA) module as an innovative token mixer within the CLB, designed to effectively handle both global and local feature extraction while maintaining the computational efficiency in cross-attention for semantic segmentation tasks.

In transformer blocks, the attention modules calculate the scaled dot-product attention for queries (Q), keys (K), and values (V) using the following formula:

$$Attention(\mathbf{Q}, \mathbf{K}, \mathbf{V}) = Softmax\left(\frac{\mathbf{Q}\mathbf{K}^\top}{\sqrt{d_k}}\right)\mathbf{V}. \quad (8)$$

Here, $\sqrt{d_k}$ represents the dimension of the key embeddings.

In Self-Attention, the features used to generate the queries, keys, and values are identical (denoted as X_{qkv}) and are derived from a common input source F_i , as shown in Fig. 3 (a). In Cross-Attention, two distinct sets of features (X_q and X_{kv}) are processed, each originating from

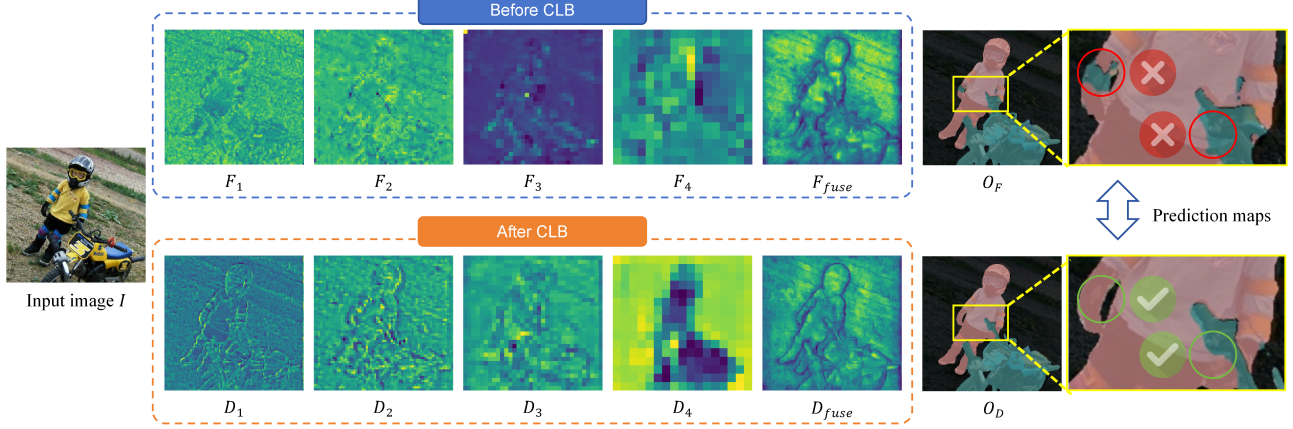


Figure 5. Visualized feature maps obtained before applying the Cross-Layer Block and after.

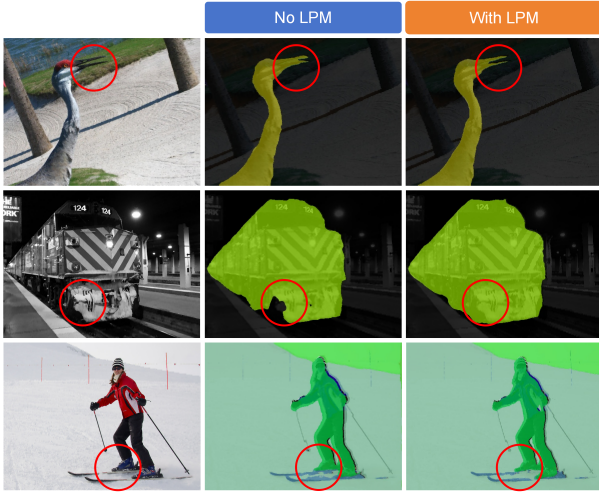


Figure 6. A visual comparison of segmentation results obtained with and without using our LPM.

a separate source, F_i and F_j , as depicted in Fig. 3 (b). In Strip Cross-Attention, a fused feature (X_{kv}) is gathered from multiple stages at different scales, denoted as M_i . This design enables the query to identify matches across multiple stages with varying levels of contextual granularity, thus supporting improved feature refinement. From an efficiency perspective, we strategically designed strip-shape tokens to implement the attention map. The channel dimensions of the original query and key are embedded into a single dimension, further reducing computational overhead. This one-dimensional transformation significantly reduces computational complexity. The computational costs of Self-Attention and Strip Cross-Attention are

$$\Omega(SA) = N^2 \cdot C + N^2 \cdot C, \quad (9)$$

and

$$\Omega(SCA) = N^2 \cdot 1 + N^2 \cdot C, \quad (10)$$

where N represents the total number of tokens.

Motivated by MetaSeg [20], we observed that the channel-compressed feature token query Q and key K , with $Q, K \in \mathbb{R}^{B \times heads \times N \times 1}$, are effective at capturing global similarities. The SCA operation is expressed as follows:

$$Q_i = W_i^Q(F_i) \in \mathbb{R}^{B \times heads \times N_i \times 1}, \quad (11)$$

$$K_i = W_i^K(M_i) \in \mathbb{R}^{B \times heads \times N_i^m \times 1}, \quad (12)$$

$$V_i = W_i^V(M_i) \in \mathbb{R}^{B \times heads \times N_i^m \times dim_{head}}, \quad (13)$$

$$Attn(Q_i, K_i) = Softmax\left(\frac{Q_i K_i^T}{\sqrt{d_k}}\right) \in \mathbb{R}^{B \times heads \times N_i \times N_i^m}, \quad (14)$$

$$P_i = Attn(Q_i, K_i) V_i^T \in \mathbb{R}^{B \times heads \times N_i \times dim_{head}}, \quad (15)$$

$$SCA(F_i, M_i) = W_i^O(cat(P_0, \dots, P_{heads})) \in \mathbb{R}^{B, N_i, C_i}, \quad (16)$$

where W_i^Q , W_i^K and W_i^V are transformation matrices used to map features, B denotes the batch size, $heads$ represents the number of attention heads, N is the number of tokens, and dim_{head} is the dimension of each head.

3.4. Local Perception Module (LPM)

Global attention is effective at capturing long-range dependencies, but it often neglects local context. To address the lack of local perception in standard self-attention and cross-attention mechanisms, we introduced a Local Perception Module (LPM) in the CLB, drawing inspiration from backbones such as XCiT [1], SMT [24], and CMT [15]. As shown in Fig. 4, the LPM can be derived using the following equation:

$$x_d = DWConv_{3 \times 3}(\sigma(DWConv_{1 \times 1}(x))), \quad (17)$$

$$\omega = Sigmoid(LN(\sigma(LN(AvgPool(x_d))))) , \quad (18)$$

$$y = x + DWConv_{1 \times 1}(\omega \odot x_d), \quad (19)$$

where $DWConv$ denotes a depthwise separable convolution, σ represents the ReLU activation function, and \odot symbolizes element-wise multiplication by channel.

Table 1. Performance comparison with SOTA light-weight models on ADE20K [53] and Cityscapes [11].

Method	Year	Backbone	Params. (M)↓	ADE20K [53]		Cityscapes [11]	
				GFLOPs↓	mIoU (%)↑	GFLOPs↓	mIoU (%)↑
SegFormer [38]	2021 NeurIPS	MiT-B0	3.8	8.4	37.4	125.5	76.2
SeaFormer [34]	2023 ICLR	SeaFormer-S	4.0	1.1	38.1	-	76.1
FeedFormer [31]	2023 AAAI	MiT-B0	4.5	7.8	39.2	107.4	77.9
U-MixFormer [44]	2023 arxiv	MiT-B0	6.1	6.1	41.2	101.7	79.0
SCTNet [41]	2024 AAAI	SCTNet-S	4.7	-	37.7	-	72.8
SDPT [4]	2024 TITS	SDPT-Tiny	3.6	5.7	39.4	63.4	77.3
PEM [5]	2024 CVPR	STDC1	17.0	16.0	39.6	92.0	78.3
MetaSeg [20]	2024 WACV	MiT-B0	4.1	3.9	37.9	90.9	76.7
vwformer [43]	2024 ICLR	MiT-B0	3.7	5.8	38.9	172.0	77.2
SCASeg (Ours)	2024	MiT-B0	6.0	5.9	41.6	101.7	79.3
SegFormer [38]	2021 NeurIPS	LVT	3.9	10.6	39.3	140.9	77.6
FeedFormer [31]	2023 AAAI	LVT	4.6	10.0	41.0	124.6	78.6
U-MixFormer [44]	2023 arxiv	LVT	6.5	9.1	43.7	122.1	79.9
MetaSeg [20]	2024 WACV	LVT	4.2	6.0	40.8	106.0	78.1
vwformer [43]	2024 ICLR	LVT	5.3	14.3	42.3	194.0	78.9
SCASeg (Ours)	2024	LVT	6.3	8.8	43.8	122.4	79.7
SegNeXt [16]	2022 NeurIPS	MSCAN-T	4.3	6.6	41.1	56.0	79.8
FeedFormer [31]	2023 AAAI	MSCAN-T	5.0	9.3	43.0	61.1	80.6
U-MixFormer [44]	2023 arxiv	MSCAN-T	6.7	7.6	44.4	54.8	81.0
MetaSeg [20]	2024 WACV	MSCAN-T	4.7	5.5	42.4	47.9	80.1
PEM [5]	2024 CVPR	STDC2	21.0	19.3	45.0	118.0	79.0
vwformer [43]	2024 ICLR	MSCAN-T	5.8	13.6	42.5	125.0	80.3
SCASeg (Ours)	2024	MSCAN-T	6.5	7.4	44.5	54.8	81.2

4. Experiments

4.1. Experimental Settings

Datasets: We conducted experiments on four benchmark datasets: ADE20K [53], Cityscapes [11], COCO-Stuff 164K [3], and PASCAL VOC2012 [18]. ADE20K [53] contains 150 semantic categories, with 20,210 training images, 2,000 validation images, and 3,352 test images. Cityscapes [11] focuses on urban scenes with 19 categories, including 2,975 training images, 500 validation images, and 1,525 test images. COCO-Stuff164K [3] has 164,000 images annotated with 171 categories, enhancing the COCO dataset with detailed scene parsing. PASCAL VOC2012 [18] includes 11,530 images across 20 categories, with pixel-level annotations.

Implementation Details: We utilized the *mmsegmentation* [10] codebase (Version 1.2.2) to train our model on eight A100 GPUs. We employed LVT, MiT-B0~5, and MSCAN as the backbone networks, while the decoder was an independently designed novel module to ensure a fair comparison. Throughout the training process, we applied common data augmentation techniques, including random horizontal flipping, random scaling with ratios ranging from 0.5 to 2.0, and random cropping to a size of 512×512 for the ADE20K, COCO-Stuff 164K, and PASCAL VOC2012 datasets, and 1024×1024 for Cityscapes. We used the AdamW optimizer to train the models for 160K iterations. For the ADE20K, COCO-Stuff 164K, and PASCAL VOC2012 datasets, the batch size was set to 16, while for Cityscapes, it was set to 8. The learning rate was initialized

at 6e-5, and a polynomial learning rate decay schedule with a factor of 1.0 was applied. We presented all of our primary semantic segmentation results using mean Intersection over Union (mIoU) in the single-scale inference setup.

4.2. Experimental Results

The main results for ADE20K and Cityscapes are shown in Table 1. For COCO-Stuff 164K and PASCAL VOC2012, we conducted fair comparisons based on the same backbone networks, with the key results presented in Table 2.

ADE20K & Cityscapes: We present the performance of the lightweight models in Table 1. As indicated in the table, our lightweight model, SCASeg (MiT-B0), achieved an mIoU of 41.6% on ADE20K, utilizing only 6.0 million parameters and 5.9 GFLOPs. In comparison to Segformer [38] (MiT-B0), SCASeg (MiT-B0) achieves a 4.2% improvement in mIoU while reducing computational cost by 29.7%. Although SDPT-Tiny [4] and vwformer [42] (MiT-B0) have a slight advantage in parameter count, their mIoU is at least 2.2% lower than that of our method. For Cityscapes, the performance gain becomes even more pronounced, with our model achieving a mIoU of 79.3% at just 101.7 GFLOPs. This represents a 3.1% improvement in mIoU and an 18.9% reduction in computational cost compared to Segformer [38] (MiT-B0). Similarly, with LVT and MSCAN-T as backbones, SCASeg consistently achieves near-SOTA performance.

COCO-Stuff 164K & PASCAL VOC2012: In Table 2, we compare our SCASeg model with previous methods on the COCO and PASCAL datasets. To ensure a fair as-

Table 2. Performance comparison with SOTA models on COCO-Stuff 164k [3] and PASCAL VOC2012 [18].

Method	Year	Backbone	Params. (M)↓	COCO-Stuff 164k [3]		PASCAL VOC2012 [18]		FPS (img/s)↑
				GFLOPs↓	mIoU (%)↑	GFLOPs↓	mIoU (%)↑	
Segformer [38]	2021 NeurIPS	MiT-B0	3.8	8.4	35.63	8.4	66.49	43.65
FeedFormer [31]	2023 AAAI	MiT-B0	4.5	7.8	39.03	7.8	68.49	34.80
U-MixFormer [44]	2023 arxiv	MiT-B0	6.1	6.1	40.24	6.1	71.16	38.94
MetaSeg [20]	2024 WACV	MiT-B0	4.1	3.9	-	3.9	68.72	42.64
vwformer [43]	2024 ICLR	MiT-B0	3.7	5.8	36.28	5.8	70.58	39.63
SCASeg (Ours)	2024	MiT-B0	6.0	5.9	40.56	5.9	72.35	40.25
SegNeXt [16]	2022 NeurIPS	MSCAN-T	4.3	6.6	38.70	6.6	76.27	33.16
FeedFormer [31]	2023 AAAI	MSCAN-T	5.0	9.3	39.39	9.3	74.80	25.98
U-MixFormer [44]	2023 arxiv	MSCAN-T	6.7	7.6	40.04	7.6	77.77	27.69
MetaSeg [20]	2024 WACV	MSCAN-T	4.7	5.5	39.70	5.5	74.98	31.74
vwformer [43]	2024 ICLR	MSCAN-T	5.8	13.6	38.85	13.6	76.53	28.06
SCASeg (Ours)	2024	MSCAN-T	6.5	7.4	40.89	7.4	77.88	29.04
SegNeXt [16]	2022 NeurIPS	MSCAN-S	13.9	15.9	41.42	15.9	78.62	30.91
FeedFormer [31]	2023 AAAI	MSCAN-S	17.6	23.6	42.61	23.6	77.42	24.16
U-MixFormer [44]	2023 arxiv	MSCAN-S	24.3	20.8	42.91	20.8	79.23	26.55
MetaSeg [20]	2024 WACV	MSCAN-S	16.3	15.3	42.13	22.5	76.73	29.83
vwformer [43]	2024 ICLR	MSCAN-S	15.5	22.5	41.76	22.5	78.95	27.37
SCASeg (Ours)	2024	MSCAN-S	23.7	20.3	43.65	20.3	79.48	27.71
Segformer [38]	2021 NeurIPS	MiT-B1	13.7	15.9	40.97	15.9	71.13	31.44
FeedFormer [31]	2023 AAAI	MiT-B1	17.3	20.7	42.42	20.7	71.77	22.29
U-MixFormer [44]	2023 arxiv	MiT-B1	24.0	17.8	42.71	17.8	74.87	22.06
MetaSeg [20]	2024 WACV	MiT-B1	16.0	12.4	42.04	12.4	73.30	27.12
vwformer [43]	2024 ICLR	MiT-B1	13.7	13.2	41.54	13.2	73.98	23.87
SCASeg (Ours)	2024	MiT-B1	23.4	17.4	43.19	17.4	75.24	25.37

assessment, we selected four backbone configurations—MiT-B0/B1 and MSCAN-T/S—and applied different methods under the same experimental conditions: 160k iterations with eight GPUs, each processing a batch size of 8. The inference time per image was tested on a V100 GPU. As observed in Table 2, our method demonstrates outstanding performance compared with other methods.

4.3. Visualization Results

Visual Comparison of Feature Maps Before and After Applying CLB: Fig. 5 presents a visual comparison of feature maps in the decoder before and after introducing the CLB. Prior to applying the CLB, features from different stages (F1–F4) lacked interaction, resulting in no exchange or complementary information between them. This limitation led to errors and inaccuracies in the segmentation results after direct fusion. However, after incorporating the CLB, it is evident that object boundaries are clearly visible at all stages, and the network demonstrates enhanced edge perception and class distinction, ultimately yielding more accurate segmentation outcomes.

Visual Comparison of Segmentation Results with and without Using LPM: The Local Perception Module (LPM) is a critical component of our design. While attention mechanisms typically emphasize global context, they often overlook local perception. By incorporating the LPM, we address this limitation. As illustrated in Fig. 6, there is a noticeable difference in the continuity of local information with and without using the LPM. For instance, objects such

as the long beak of a red-crowned crane or a snowboard are prone to misprediction due to the influence of surrounding larger objects. The LPM effectively alleviated this issue, enabling more consistent segmentation of small details.

Visual Comparison of Segmentation Results: Fig. 7 shows the visual comparison of the segmentation results obtained on the ADE20K datasets using our SCASeg and SOTA methods. The highlighted areas indicate regions where SCASeg outperforms the other methods in segmentation quality. This improvement is evident in two main aspects: first, the prediction accuracy for objects within the same category has increased (*e.g.*, the pole next to the car and the chandelier); second, boundary segmentation accuracy has improved (*e.g.*, billboards). Additionally, small objects, such as traffic lights, are detected and predicted correctly. Compared to SOTA methods, SCASeg achieves better recognition of object details near boundaries. This indicates that our model captures a more relevant visual context by leveraging the capacity of the CLB decoder strategy.

4.4. Ablation Studies

Effectiveness of Strip Cross-Attention (SCA): In Table 3, we demonstrate the effectiveness of incorporating SCA within the decoder. SCA serves as a core component of the CLB, primarily facilitating cross-level feature enhancement and interaction among different hierarchical layers. As shown in this table, incorporating self-attention in the decoder stage results in a 3.75% improvement in segmentation accuracy. Compared to Self-Attention (SA), SCA achieves

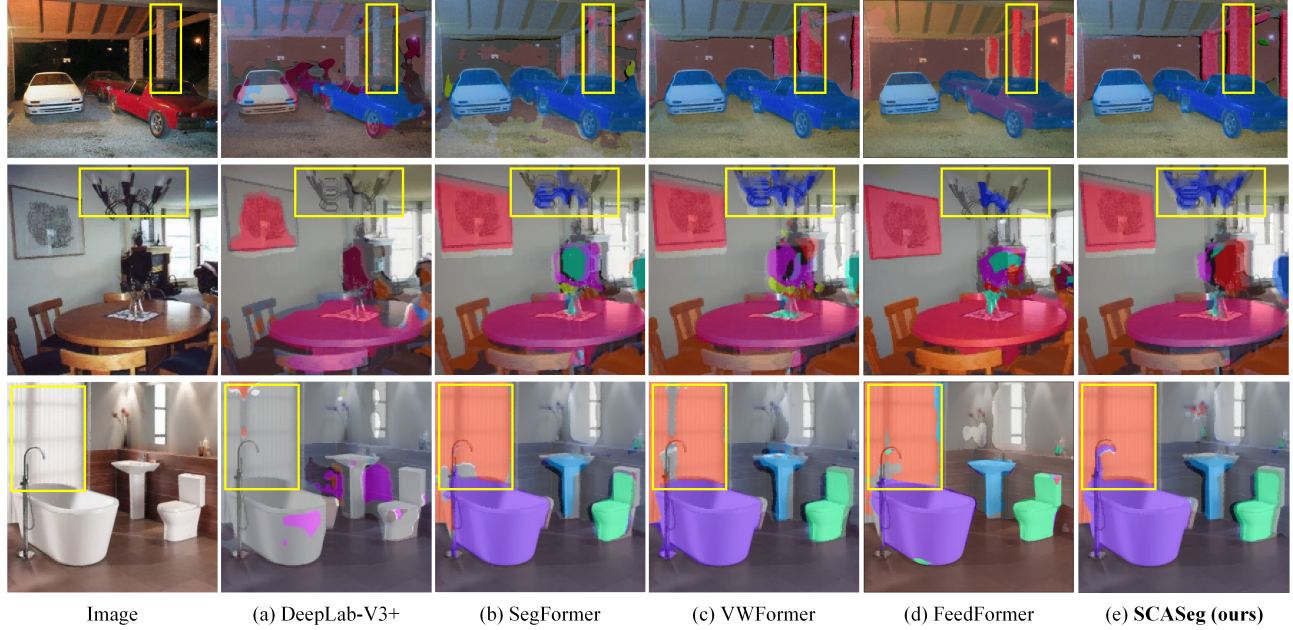


Figure 7. Visual segmentation results obtained on the ADE20K [53].

Table 3. Ablation study of SCA on PASCAL VOC2012 [18].

Method	Para.↓	GFLOPs↓	mIoU (%)↑	FPS (img/s)↑
MiT-B0	3.8 M	8.4	66.49	44.0
+ SA	4.3 M	9.0	70.06 (+3.57)	45.0
+ CA	6.0 M	5.9	71.79 (+5.30)	42.0
+ SCA	5.7 M	5.5	71.53 (+5.04)	43.0
+ SCA + LPM	6.0 M	5.9	72.39 (+5.90)	42.0
MSCAN-T	4.3 M	6.6	76.27	33.0
+ SA	4.8 M	10.4	76.92 (+0.65)	30.0
+ CA	6.7 M	7.3	77.38 (+1.11)	29.0
+ SCA	6.3 M	6.9	76.74 (+0.47)	31.0
+ SCA + LPM	6.5 M	7.4	77.88 (+1.61)	29.0

a notable reduction in computational overhead, lowering FLOPs by 38.9% while still delivering a 1.47% improvement in mIoU. Comparisons between Cross-Attention (CA) and SCA reveal that SCA not only enhances performance but also reduces parameter count by 0.3 million and computation by 0.4 GFLOPs, along with a slight advantage in inference speed. This demonstrates that SCA not only maintains high segmentation performance but also significantly enhances computational efficiency, making it a highly effective alternative for applications with limited resources.

Effectiveness of the Cross-Layer Strategy: The comparative experiments on cross-layer strategies highlight the necessity of information exchange across features at different stages. During the encoding phase, four processing stages generate features that vary in semantic richness and detail when passed to the decoder. Shallow stages, such as Stage 1 and Stage 2, retain more detailed information as they undergo less downsampling and fewer convolutional operations, resulting in clearer edge information. In contrast,

Table 4. Ablation study of cross-layer strategy on PASCAL VOC2012 [18].

Method	Cross-Layer				Para.↓	GFLOPs↓	mIoU↑
	4	3	2	1			
SCASeg (MiT-B0)	✓	✗	✗	✗	5.7 M	4.6	69.76
	✓	✓	✗	✗	5.7 M	4.9	70.68
	✓	✓	✓	✗	5.7 M	5.2	71.16
	✓	✓	✓	✓	6.0 M	5.9	72.35
SCASeg (MSCAN-T)	✓	✗	✗	✗	6.3 M	6.0	75.73
	✓	✓	✗	✗	6.3 M	6.3	76.32
	✓	✓	✓	✗	6.3 M	6.6	76.84
	✓	✓	✓	✓	6.5 M	7.4	77.88

deeper stages, such as Stage 3 and Stage 4, capture richer contextual information due to more extensive feature abstraction. As shown in Table 4, applying the CLB module across all four stages and enabling cross-layer operations significantly boosts segmentation performance (72.35% for MiT-B0, 77.88% for MSCAN-T). This improvement underscores the effectiveness and necessity of cross-layer operations in achieving high segmentation accuracy.

5. Conclusion

This paper presents a novel decoder design, SCASeg, which incorporates a Strip Cross-Layer Block. Extensive experiments conducted on four benchmark datasets demonstrate that SCASeg’s versatile decoder consistently achieves SOTA performance across various configurations, outperforming existing segmentation architectures on all four benchmarks. These results highlight the importance of designing decoders tailored to specific tasks, such as semantic segmentation, to enhance both performance and computational efficiency, alongside optimizing the encoder.

References

- [1] Alaaeldin Ali, Hugo Touvron, Mathilde Caron, Piotr Bojanowski, Matthijs Douze, Armand Joulin, Ivan Laptev, Natalia Neverova, Gabriel Synnaeve, Jakob Verbeek, et al. Xcit: Cross-covariance image transformers. *Advances in Neural Information Processing Systems*, 34:20014–20027, 2021. 2, 5
- [2] Reza Azad, Ehsan Khodapanah Aghdam, Amelie Rauland, Yiwei Jia, Atlas Haddadi Avval, Afshin Bozorgpour, Sanaz Karimijafarbigloo, Joseph Paul Cohen, Ehsan Adeli, and Dorit Merhof. Medical image segmentation review: The success of u-net. *IEEE Transactions on Pattern Analysis and Machine Intelligence*, 46(12):10076–10095, 2024. 1
- [3] Holger Caesar, Jasper Uijlings, and Vittorio Ferrari. Cocomp: Thing and stuff classes in context. In *CVPR*, pages 1209–1218, 2018. 6, 7
- [4] Hu Cao, Guang Chen, Hengshuang Zhao, Dongsheng Jiang, Xiaopeng Zhang, Qi Tian, and Alois Knoll. Sdpt: Semantic-aware dimension-pooling transformer for image segmentation. *IEEE Transactions on Intelligent Transportation Systems*, 25(11):15934–15946, 2024. 6
- [5] Niccolò Cavagnero, Gabriele Rosi, Claudia Cuttano, Francesca Pistilli, Marco Ciccone, Giuseppe Averta, and Fabio Cermelli. Pem: Prototype-based efficient maskformer for image segmentation. In *CVPR*, pages 15804–15813, 2024. 6, 1, 2
- [6] Liang-Chieh Chen, George Papandreou, Florian Schroff, and Hartwig Adam. Rethinking atrous convolution for semantic image segmentation. *arXiv preprint arXiv:1706.05587*, 2017. 2
- [7] Liang-Chieh Chen, Yukun Zhu, George Papandreou, Florian Schroff, and Hartwig Adam. Encoder-decoder with atrous separable convolution for semantic image segmentation. In *ECCV*, pages 801–818, 2018. 2
- [8] Bowen Cheng, Alex Schwing, and Alexander Kirillov. Per-pixel classification is not all you need for semantic segmentation. *Advances in Neural Information Processing Systems*, 34:17864–17875, 2021. 1, 3
- [9] Bowen Cheng, Ishan Misra, Alexander G Schwing, Alexander Kirillov, and Rohit Girdhar. Masked-attention mask transformer for universal image segmentation. In *CVPR*, pages 1290–1299, 2022. 2
- [10] MMSegmentation Contributors. MMSegmentation: Openmmlab semantic segmentation toolbox and benchmark. <https://github.com/open-mmlab/mms Segmentation>, 2020. 6
- [11] Marius Cordts, Mohamed Omran, Sebastian Ramos, Timo Rehfeld, Markus Enzweiler, Rodrigo Benenson, Uwe Franke, Stefan Roth, and Bernt Schiele. The cityscapes dataset for semantic urban scene understanding. In *CVPR*, pages 3213–3223, 2016. 6, 2, 3, 4
- [12] Henghui Ding, Xudong Jiang, Ai Qun Liu, Nadia Magnenat Thalmann, and Gang Wang. Boundary-aware feature propagation for scene segmentation. In *ICCV*, pages 6819–6829, 2019. 2
- [13] Alexey Dosovitskiy, Lucas Beyer, Alexander Kolesnikov, Dirk Weissenborn, Xiaohua Zhai, Thomas Unterthiner, Mostafa Dehghani, Matthias Minderer, Georg Heigold, Sylvain Gelly, et al. An image is worth 16x16 words: Transformers for image recognition at scale. *arXiv preprint arXiv:2010.11929*, 2020. 1
- [14] Jun Fu, Jing Liu, Haijie Tian, Yong Li, Yongjun Bao, Zhiwei Fang, and Hanqing Lu. Dual attention network for scene segmentation. In *CVPR*, pages 3146–3154, 2019. 1, 2
- [15] Jianyuan Guo, Kai Han, Han Wu, Yehui Tang, Xinghao Chen, Yunhe Wang, and Chang Xu. Cmt: Convolutional neural networks meet vision transformers. In *CVPR*, pages 12175–12185, 2022. 2, 5
- [16] Meng-Hao Guo, Cheng-Ze Lu, Qibin Hou, Zhengning Liu, Ming-Ming Cheng, and Shi-Min Hu. Segnext: Rethinking convolutional attention design for semantic segmentation. *Advances in Neural Information Processing Systems*, 35:1140–1156, 2022. 1, 2, 6, 7, 3
- [17] Junjun He, Zhongying Deng, Lei Zhou, Yali Wang, and Yu Qiao. Adaptive pyramid context network for semantic segmentation. In *CVPR*, pages 7519–7528, 2019. 2
- [18] Derek Hoiem, Santosh K Divvala, and James H Hays. Pascal voc 2008 challenge. *World Literature Today*, 24(1):1–4, 2009. 6, 7, 8, 3
- [19] Zilong Huang, Xinggang Wang, Lichao Huang, Chang Huang, Yunchao Wei, and Wenyu Liu. Ccnet: Criss-cross attention for semantic segmentation. In *ICCV*, pages 603–612, 2019. 2
- [20] Beoungwoo Kang, Seunghun Moon, Yubin Cho, Hyunwoo Yu, and Suk-Ju Kang. Metaseg: Metaformer-based global contexts-aware network for efficient semantic segmentation. In *WACV*, pages 434–443, 2024. 2, 5, 6, 7, 1, 3
- [21] Alexander Kirillov, Eric Mintun, Nikhila Ravi, Hanzi Mao, Chloe Rolland, Laura Gustafson, Tete Xiao, Spencer Whitehead, Alexander C Berg, Wan-Yen Lo, et al. Segment anything. In *ICCV*, pages 4015–4026, 2023. 1
- [22] Xin Lai, Zhuotao Tian, Yukang Chen, Yanwei Li, Yuhui Yuan, Shu Liu, and Jiaya Jia. Lisa: Reasoning segmentation via large language model. In *CVPR*, pages 9579–9589, 2024. 1
- [23] Chen Liang-Chieh, George Papandreou, Iasonas Kokkinos, Kevin Murphy, and Alan Yuille. Semantic image segmentation with deep convolutional nets and fully connected crfs. In *ICLR*, 2015. 2
- [24] Weifeng Lin, Ziheng Wu, Jiayu Chen, Jun Huang, and Lianwen Jin. Scale-aware modulation meet transformer. In *ICCV*, pages 6015–6026, 2023. 2, 5
- [25] Chenxi Liu, Liang-Chieh Chen, Florian Schroff, Hartwig Adam, Wei Hua, Alan L Yuille, and Li Fei-Fei. Auto-deeplab: Hierarchical neural architecture search for semantic image segmentation. In *CVPR*, pages 82–92, 2019. 2
- [26] Liyang Liu, Zihan Wang, Minh Hieu Phan, Bowen Zhang, Jinchao Ge, and Yifan Liu. Bpkd: Boundary privileged knowledge distillation for semantic segmentation. In *WACV*, pages 1062–1072, 2024. 2
- [27] Jonathan Long, Evan Shelhamer, and Trevor Darrell. Fully convolutional networks for semantic segmentation. In *CVPR*, pages 3431–3440, 2015. 1, 2

- [28] Xu Ma, Xiyang Dai, Jianwei Yang, Bin Xiao, Yinpeng Chen, Yun Fu, and Lu Yuan. Efficient modulation for vision networks. *arXiv preprint arXiv:2403.19963*, 2024. 1, 2
- [29] Chao Peng, Xiangyu Zhang, Gang Yu, Guiming Luo, and Jian Sun. Large kernel matters—improve semantic segmentation by global convolutional network. In *CVPR*, pages 4353–4361, 2017. 2
- [30] Bowen Shi, Dongsheng Jiang, Xiaopeng Zhang, Han Li, Wenrui Dai, Junni Zou, Hongkai Xiong, and Qi Tian. A transformer-based decoder for semantic segmentation with multi-level context mining. In *ECCV*, pages 624–639. Springer, 2022. 1, 2
- [31] Jae-hun Shim, Hyunwoo Yu, Kyeongbo Kong, and Suk-Ju Kang. Feedformer: Revisiting transformer decoder for efficient semantic segmentation. In *AAAI*, pages 2263–2271, 2023. 2, 6, 7, 1, 3
- [32] Robin Strudel, Ricardo Garcia, Ivan Laptev, and Cordelia Schmid. Segmenter: Transformer for semantic segmentation. In *ICCV*, pages 7262–7272, 2021. 2, 3
- [33] Ashish Vaswani, Noam Shazeer, Niki Parmar, Jakob Uszkoreit, Llion Jones, Aidan N Gomez, Łukasz Kaiser, and Illia Polosukhin. Attention is all you need. *Advances in Neural Information Processing Systems*, 30:1–11, 2017. 1
- [34] Qiang Wan, Zilong Huang, Jiachen Lu, YU Gang, and Li Zhang. Seaformer: Squeeze-enhanced axial transformer for mobile semantic segmentation. In *ICLR*, 2023. 6, 2
- [35] Di Wang, Jing Zhang, Bo Du, Mingqiang Xu, Lin Liu, Dacheng Tao, and Liangpei Zhang. Samrs: Scaling-up remote sensing segmentation dataset with segment anything model. *Advances in Neural Information Processing Systems*, 36, 2024. 1
- [36] Xiaolong Wang, Ross Girshick, Abhinav Gupta, and Kaiming He. Non-local neural networks. In *CVPR*, pages 7794–7803, 2018. 2
- [37] Chunlong Xia, Xinliang Wang, Feng Lv, Xin Hao, and Yifeng Shi. Vit-comer: Vision transformer with convolutional multi-scale feature interaction for dense predictions. In *CVPR*, pages 5493–5502, 2024. 2, 3
- [38] Enze Xie, Wenhui Wang, Zhiding Yu, Anima Anandkumar, Jose M Alvarez, and Ping Luo. Segformer: Simple and efficient design for semantic segmentation with transformers. *Advances in Neural Information Processing Systems*, 34:12077–12090, 2021. 2, 6, 7, 3
- [39] Guoan Xu, Juncheng Li, Guangwei Gao, Huimin Lu, Jian Yang, and Dong Yue. Lightweight real-time semantic segmentation network with efficient transformer and cnn. *IEEE Transactions on Intelligent Transportation Systems*, 24(12): 15897–15906, 2023. 1
- [40] Guoan Xu, Wenfeng Huang, Tao Wu, Ligeng Chen, Wenjing Jia, Guangwei Gao, Xiatian Zhu, and Stuart Perry. Macformer: Semantic segmentation with fine object boundaries. *arXiv preprint arXiv:2408.05699*, 2024. 2, 1
- [41] Zhengze Xu, Dongyue Wu, Changqian Yu, Xiangxiang Chu, Nong Sang, and Changxin Gao. Sctnet: Single-branch cnn with transformer semantic information for real-time segmentation. In *AAAI*, pages 6378–6386, 2024. 2, 6
- [42] Haotian Yan, Ming Wu, and Chuang Zhang. Multi-scale representations by varying window attention for semantic segmentation. In *ICLR*, 2024. 6
- [43] Haotian Yan, Ming Wu, and Chuang Zhang. Multi-scale representations by varying window attention for semantic segmentation. In *ICLR*, 2024. 6, 7, 2, 3
- [44] Seul-Ki Yeom and Julian von Klitzing. U-mixformer: Unet-like transformer with mix-attention for efficient semantic segmentation. *arXiv preprint arXiv:2312.06272*, 2023. 2, 3, 6, 7, 1
- [45] Changqian Yu, Jingbo Wang, Changxin Gao, Gang Yu, Chunhua Shen, and Nong Sang. Context prior for scene segmentation. In *CVPR*, pages 12416–12425, 2020. 2
- [46] Weihao Yu, Mi Luo, Pan Zhou, Chenyang Si, Yichen Zhou, Xinchao Wang, Jiashi Feng, and Shuicheng Yan. Metaformer is actually what you need for vision. In *CVPR*, pages 10819–10829, 2022. 2, 4
- [47] Yuhui Yuan, Xilin Chen, and Jingdong Wang. Object-contextual representations for semantic segmentation. In *ECCV*, pages 173–190. Springer, 2020. 1, 2
- [48] Yuhui Yuan, Jingyi Xie, Xilin Chen, and Jingdong Wang. Segfix: Model-agnostic boundary refinement for segmentation. In *ECCV*, pages 489–506. Springer, 2020. 2
- [49] Hang Zhang, Kristin Dana, Jianping Shi, Zhongyue Zhang, Xiaogang Wang, Amrith Tyagi, and Amit Agrawal. Context encoding for semantic segmentation. In *CVPR*, pages 7151–7160, 2018. 1, 2
- [50] Mingmin Zhen, Jinglu Wang, Lei Zhou, Shiwei Li, Tianwei Shen, Jiayang Shang, Tian Fang, and Long Quan. Joint semantic segmentation and boundary detection using iterative pyramid contexts. In *CVPR*, pages 13666–13675, 2020. 2
- [51] Sixiao Zheng, Jiachen Lu, Hengshuang Zhao, Xiatian Zhu, Zekun Luo, Yabiao Wang, Yanwei Fu, Jianfeng Feng, Tao Xiang, Philip HS Torr, et al. Rethinking semantic segmentation from a sequence-to-sequence perspective with transformers. In *CVPR*, pages 6881–6890, 2021. 2, 3
- [52] Zilong Zhong, Zhong Qiu Lin, Rene Bidart, Xiaodan Hu, Ibrahim Ben Daya, Zhifeng Li, Wei-Shi Zheng, Jonathan Li, and Alexander Wong. Squeeze-and-attention networks for semantic segmentation. In *CVPR*, pages 13065–13074, 2020. 2
- [53] Bolei Zhou, Hang Zhao, Xavier Puig, Sanja Fidler, Adela Barriuso, and Antonio Torralba. Scene parsing through ade20k dataset. In *CVPR*, pages 633–641, 2017. 1, 6, 8, 2, 3

SCASeg: Strip Cross-Attention for Efficient Semantic Segmentation

Supplementary Material

This supplementary document provides additional insights and experimental results to complement the main paper. First, we present an in-depth analysis of the CLB module, highlighting its contributions to the overall performance. Next, we compare our method with medium-weight and heavy-weight models to demonstrate its effectiveness across different model complexities. Additionally, we include further visual experiment results to showcase the qualitative improvements achieved by our approach. Finally, we provide additional ablation studies to thoroughly evaluate the impact of various components and design choices in our framework.

1. Relationship of CLB with Existing Attention Blocks

In the main paper, we introduced a Cross-Layer Block (CLB) that blends hierarchical feature maps from different encoder and decoder stages to create a unified representation for Keys and Values. In this Supplementary, we illustrate the relationship of the proposed Cross-Layer Block (CLB) to other SOTA attention blocks, as shown in Fig. 8.

These works introduce various modifications to the self-attention block, with a focus on enhancing the token-mixer component. Examples include MetaSeg’s [20] channel-wise compression of Q and K , Feedformer’s [31] feature-wise interactions, U-Mixformer’s [44] balanced approach, and MacFormer’s [40] bidirectional design. However, these methods often prioritize one aspect over others, resulting in limitations regarding feature interactions, computational cost, or local context preservation. In contrast, CLB effectively addresses these challenges by integrating the advantages of cross-layer fusion, local context retention, and computational efficiency.

2. Additional Experimental Comparisons with Medium-weight and Heavy-weight Models

In the main paper, we compared the performance of the SCASeg (MiT-B0) with lightweight models. In this Supplementary, we present additional experimental comparison conducted with medium-weight and heavy-weight models on ADE20K and Cityscapes.

2.1. Medium-weight Models:

As presented in Table 5, our SCASeg demonstrates superior performance compared to other methods when paired with equivalent heavy encoders. SCASeg (MiT-B1) achieved a mIoU of 45.4% on ADE20K, utilizing just 23.4 million

parameters and 17.4 GFLOPs. With MiT-B1 as the backbone, our approach achieves a 15.9% reduction in GFLOPs while improving performance by 1.2% compared to FeedFormer [31]. The PEM model [5], which exhibits similar performance (45.5% vs. 45.4%), contains 52% more parameters and requires 2.7 times the GFLOPs (46.9 vs. 17.4) of our method. Although EfficientMod [28] achieves a mIoU that is 0.6% higher than ours, it incurs an additional computational cost of nearly 11 GFLOPs. For the Cityscapes dataset, we achieved a SOTA segmentation accuracy of 80.3%. Similarly, when comparing networks using MSCAN-S and MiT-B2 as backbones, our method effectively balances performance and efficiency.

2.2. Heavyweight models:

Table 6 presents the experimental comparison using heavy backbones, specifically MSCAN-B and MiT-B3/4/5. Our method also demonstrates solid results. For instance, on the ADE20K dataset, SCASeg (MSCAN-B) achieves a mIoU of 49.6% with only 33.5 GFLOPs. In comparison, the similar U-Mixformer [44] shows similar performance with more parameters and computation. For the Cityscapes dataset, using MiT-B5 as the backbone, our method achieved a SOTA mIoU of 83.5%, with a relatively small and justifiable cost of 1173.0 GFLOPs. Although MetaSeg’s [20] GFLOPs are 2.6% lower than ours (1143 vs. 1173), its mIoU is 1% lower, representing a significant gap. These experimental results demonstrate that, under the same conditions, our method strikes a better balance between performance and efficiency compared to other approaches, highlighting its distinct advantages and validating its effectiveness.

3. Additional Visualization Results

Fig. 9 shows additional visual comparison of the segmentation results obtained on the Cityscapes datasets using our SCASeg and SOTA methods.

4. Additional Ablation Studies

Effectiveness of the Local Perception Module (LPM): Table 3 in the main paper also presents the results of combining SCA with LPM, forming the complete CLB structure. With the addition of LPM, the parameter count and computational load become comparable to those of CA, while this combination achieves an increase in segmentation performance of over 0.5%. Moreover, the inference speed remains nearly identical. In Table 7, we conducted a comparative experiment using SENet within LPM to enhance the model’s sensitivity to local information. When

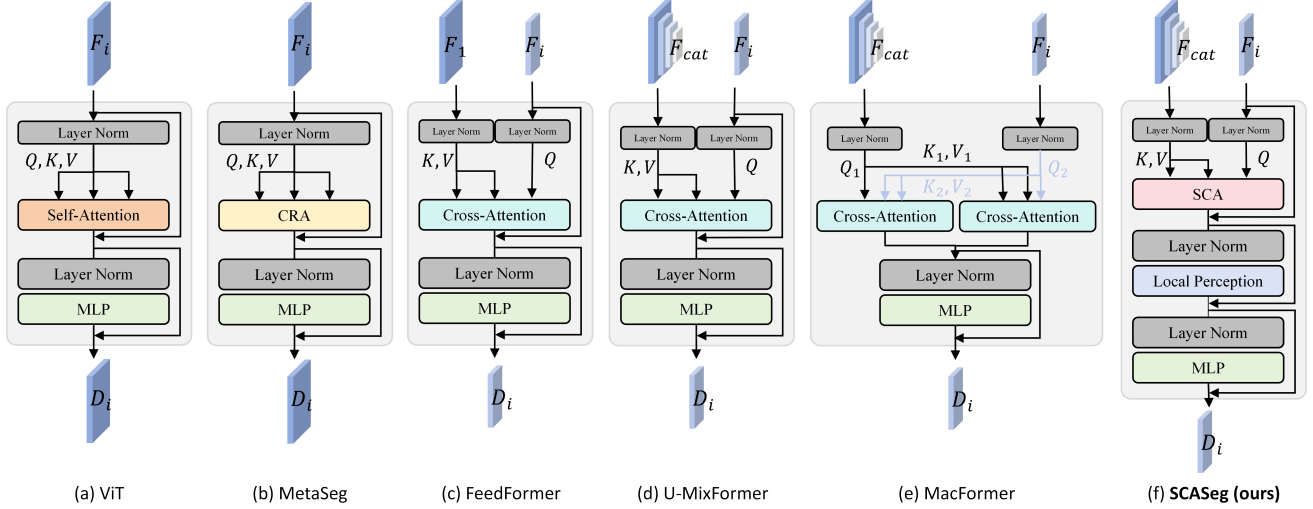


Figure 8. The Cross-Layer Block (CLB) in the proposed SCASeg compared to its counterparts in SOTA approaches.

Table 5. Performance comparison with SOTA medium-weight models on ADE20K [53] and Cityscapes [11].

Method	Year	Backbone	Params. (M)↓	ADE20K [53]		Cityscapes [11]	
				GFLOPs↓	mIoU (%)↑	GFLOPs↓	mIoU (%)↑
CCNet [19]	2019 ICCV	ResNet-101	68.9	278.4	43.7	2224.8	79.5
EncNet [49]	2018 CVPR	ResNet-101	55.1	218.8	44.7	1748.0	76.9
DeepLab-V3+ [7]	2018 ECCV	ResNet-101	52.7	255.1	44.1	2032.3	80.9
Mask2Former [9]	2022 CVPR	ResNet-101	63.0	90.0	47.8	-	-
Auto-DeepLab [25]	2019 CVPR	Auto-DeepLab-L	44.4	-	-	695.0	80.3
OCRNet [47]	2020 ECCV	HRNet-W48	70.5	164.8	45.6	1296.8	81.1
SegFormer [38]	2021 NeurIPS	MiT-B1	13.7	15.9	42.2	243.7	78.5
SegDformer [30]	2022 ECCV	MiT-B1	14.4	-	44.1	-	-
SeaFormer [34]	2023 ICLR	SeaFormer-B	8.6	1.8	40.2	-	77.7
SCTNet [41]	2024 AAAI	SCTNet-B	17.4	-	43.0	-	79.8
FeedFormer [31]	2023 AAAI	MiT-B1	17.3	20.7	44.2	256.0	79.0
U-MixFormer [44]	2023 arxiv	MiT-B1	24.0	17.8	45.2	246.8	79.9
EfficientMod [28]	2024 ICLR	EfficientMod-s	16.7	28.1	46.0	-	-
SFNet	2024 IJCV	ResNet-18	12.3	-	-	-	80.1
MetaSeg [20]	2024 WACV	MiT-B1	16.0	12.4	43.8	219.0	78.6
PEM [5]	2024 CVPR	ResNet-50	35.6	46.9	45.5	240.0	79.9
vwformer [43]	2024 ICLR	MiT-B1	13.7	13.2	43.2	289.0	79.0
SCASeg (Ours)	2024	MiT-B1	23.4	17.4	45.4	249.0	80.3
SegNeXt [16]	2022 NeurIPS	MSCAN-S	13.9	15.9	44.3	124.6	81.3
FeedFormer [31]	2023 AAAI	MSCAN-S	17.6	23.6	46.7	163.0	81.5
U-MixFormer [44]	2023 arxiv	MSCAN-S	24.3	20.8	48.4	154.0	81.8
MetaSeg [20]	2024 WACV	MSCAN-S	16.3	15.3	45.9	126.0	81.3
vwformer [43]	2024 ICLR	MSCAN-S	15.5	22.5	46.2	196.0	81.7
SCASeg (Ours)	2024	MSCAN-S	23.7	20.3	48.8	156.0	81.6
SegFormer [38]	2021 NeurIPS	MiT-B2	27.5	62.4	46.5	717.1	81.0
SegDformer [30]	2022 ECCV	MiT-B2	27.6	-	47.5	-	-
FeedFormer [31]	2023 AAAI	MiT-B2	29.1	42.7	48.0	522.7	81.5
U-MixFormer [44]	2023 arxiv	MiT-B2	35.8	40.0	48.2	515.0	81.7
MetaSeg [20]	2024 WACV	MiT-B2	27.8	25.2	46.3	420.0	81.2
vwformer [43]	2024 ICLR	MiT-B2	27.4	46.6	48.1	469.0	80.7
SCASeg (Ours)	2024	MiT-B2	35.2	39.6	48.3	517.0	81.9

compared to other channel attention mechanisms (CBAM, ECANet, CooAtt), SENet achieved the highest segmenta-

tion accuracy, outperforming CooAtt by more than 0.3%. The integration of SENet with LPM significantly strength-

Table 6. Performance comparison with SOTA heavyweight models on ADE20K [53] and Cityscapes [11].

Method	Year	Backbone	Params. (M)↓	ADE20K [53]		Cityscapes [11]	
				GFLOPs↓	mIoU (%)↑	GFLOPs↓	mIoU (%)↑
Seg-B-Mask/16 [32]	2021 ICCV	ViT-Base	106.0	-	48.5	-	-
MaskFormer [8]	2021 NeurIPS	Swin-S	63.0	79.0	49.8	-	-
SETR [51]	2021 CVPR	ViT-Large	318.3	-	50.2	-	82.2
SegNeXt [16]	2022 NeurIPS	MSCAN-B	27.6	34.9	48.5	275.7	82.6
FeedFormer [31]	2023 AAAI	MSCAN-B	30.5	36.8	48.3	269.0	82.1
U-MixFormer [44]	2023 arxiv	MSCAN-B	37.2	34.0	49.5	259.0	83.2
MetaSeg [20]	2024 WACV	MSCAN-B	29.6	30.4	48.5	251.1	82.7
vwformer [43]	2024 ICLR	MSCAN-B	28.3	35.7	48.1	302.0	82.3
SCASeg (Ours)	2024	MSCAN-B	36.5	33.5	49.6	261.0	83.0
SegFormer [38]	2021 NeurIPS	MiT-B3	47.3	79.0	49.4	962.9	81.7
FeedFormer [31]	2023 AAAI	MiT-B3	48.3	47.2	49.5	682.0	81.9
U-MixFormer [44]	2023 arxiv	MiT-B3	55.7	56.8	49.8	673.0	82.9
MetaSeg [20]	2024 WACV	MiT-B3	47.7	41.8	48.7	645.0	81.8
vwformer [43]	2024 ICLR	MiT-B3	47.3	63.3	49.6	715.0	82.4
SCASeg (Ours)	2024	MiT-B3	55.1	56.3	50.1	675.0	83.0
SegFormer [38]	2021 NeurIPS	MiT-B4	64.1	95.7	50.3	1240.6	82.3
FeedFormer [31]	2023 AAAI	MiT-B4	65.0	63.8	50.7	960.0	82.6
U-MixFormer [44]	2023 arxiv	MiT-B4	72.4	73.4	50.8	951.0	82.9
MetaSeg [20]	2024 WACV	MiT-B4	63.6	55.5	50.5	923.0	82.1
vwformer [43]	2024 ICLR	MiT-B4	64.0	79.9	50.1	993.0	82.7
SCASeg (Ours)	2024	MiT-B4	71.8	72.9	50.9	953.0	83.2
SegFormer [38]	2021 NeurIPS	MiT-B5	84.7	183.3	51.0	1460.4	82.4
FeedFormer [31]	2023 AAAI	MiT-B5	85.6	79.8	51.2	1180.0	82.7
U-MixFormer [44]	2023 arxiv	MiT-B5	93.0	149.5	51.9	1171.0	83.1
ViT-CoMer [37]	2024 CVPR	ViT-CoMer-B	144.7	-	48.8	-	-
ViT-CoMer [37]	2024 CVPR	ViT-CoMer-L	383.4	-	54.3	-	-
MetaSeg [20]	2024 WACV	MiT-B5	85.0	74.5	51.4	1143.0	82.5
vwformer [43]	2024 ICLR	MiT-B5	84.6	96.1	52.0	1213.0	82.8
SCASeg (Ours)	2024	MiT-B5	92.4	88.9	52.7	1173.0	83.5

Table 7. Ablation study of Local Perception Module (LPM) on PASCAL VOC2012 [18] dataset.

Method	Param. (M)↓	GFLOPs↓	mIoU (%)↑
SCA (MiT-B0)	5.7	5.5	71.53
+ LPM (CBAM)	5.9	5.7	71.29 (-0.24)
+ LPM (ECANet)	5.9	5.7	71.58 (+0.05)
+ LPM (CooAtt)	6.0	5.7	71.87 (+0.34)
+ LPM (SENet)	6.0	5.9	72.39 (+0.86)
SCA (MSCAN-T)	6.3	6.9	76.74
+ LPM (CBAM)	6.5	7.1	76.79 (+0.05)
+ LPM (ECANet)	6.5	7.1	76.49 (-0.25)
+ LPM (CooAtt)	6.5	7.1	77.57 (+0.83)
+ LPM (SENet)	6.5	7.4	77.88 (+1.14)

ens the model’s ability to model local features, enhancing coherence in segmentation and reducing misclassification of small objects or local regions of the same class.

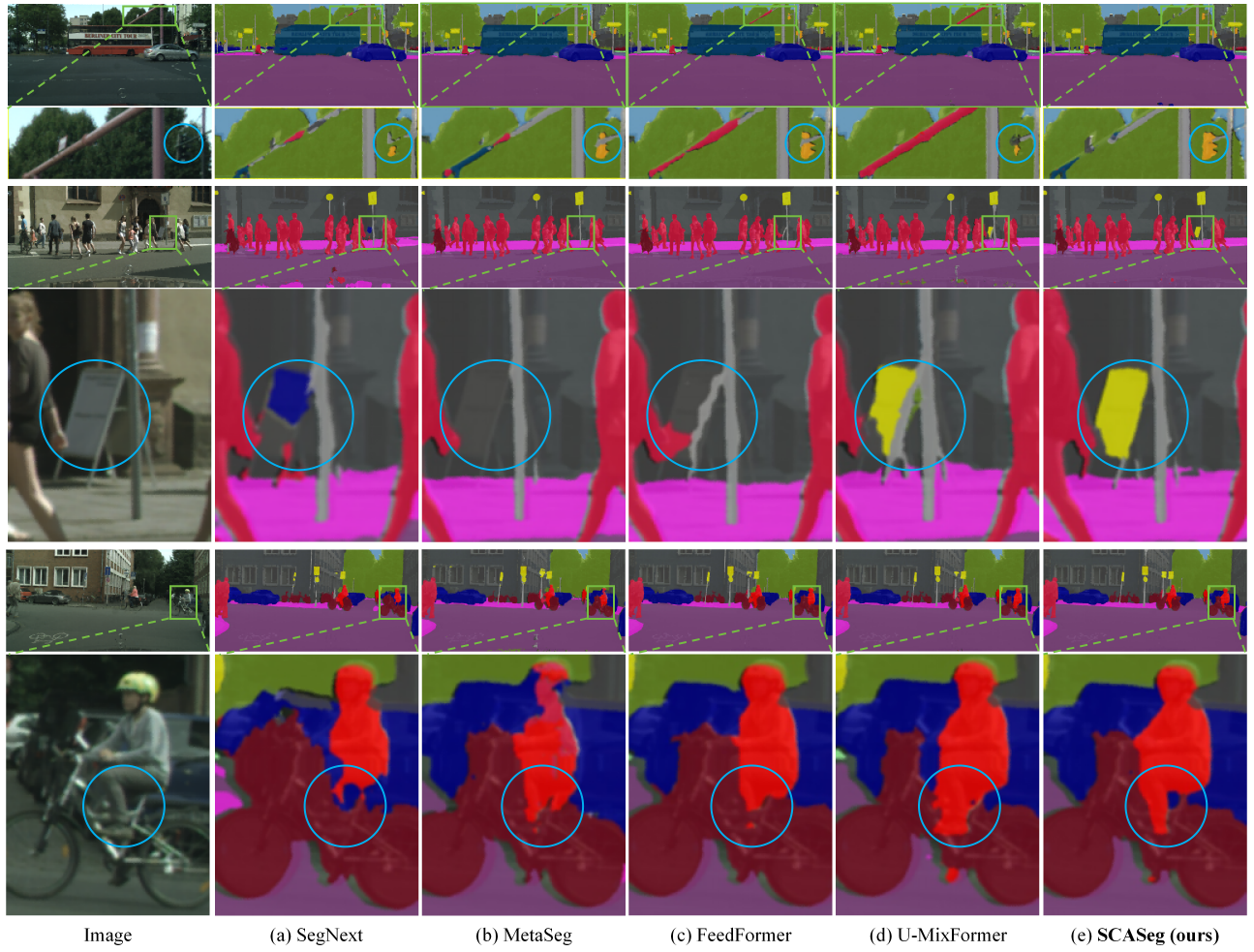


Figure 9. Visual segmentation results obtained on the Cityscapes [11] dataset.